11th International Symposium on Magnetic Bearings
August 26-29, Nara, Japan

A MODEL OF MAGNETIC RELUCTANCE OF CYLINDRICAL SOLID IRON-CORES

Satoru Fukata
Faculty of Design, Kyushu University, Mimamiku, Fukuoka 815-8540, Japan
fukata@design.kyushu-u.ac.jp

ABSTRACT
A model of magnetic reluctance is considered in the frequency domain for cylindrical solid iron-cores when magnetic flux normally enters and leaves on the circumferential surface. To have an analytical model, we take a iron core that is sufficiently high to spread the magnetic flux over the circumferential surface and not out over the upper and lower ends. First, a three-dimensional distribution of the magnetic field is solved with Laplace transform. Then, the magnetomotive force between the two pole faces is obtained by a mean value along flux paths on the surface to describe the magnetic reluctance. The model given by Bessel functions is approximated in a simple form. The numerical result is compared with an experimental result to check the applicability of the model to actual cores.

INTRODUCTION
It is simple to apply the magnetic circuit theory to the dynamical model of magnetic actuators if the magnetic reluctances of the iron cores are known. In the actuators used for magnetic radial bearings, the magnet iron cores, for example, consist of a C-shaped core (stator) wound with magnet coils and a cylindrical core (rotor). It may be applicable a rectangular core model to the stator core [1,2]; but no model has presented to the rotor core.

The height (axial length) of the rotor core is near that of the stator core (the former may be slightly higher than the latter). Hence, the magnetic flux dynamically spreads over the upper and lower ends beyond the circumferential surface of the rotor core. For such a case, it seems difficult to obtain an analytical model of the magnetic reluctance; this is why we should consider the boundary conditions on both the circumferential surface and the upper and lower ends of the core. An analytical solution, however, may be possible without the ends.

Some experimental data show that the dynamic characteristics have little difference between the higher and lower cores. We can conclude that this fact is due to a similar effect of the ends to the circumferential surface. Hence, if we can obtain a model for an iron core sufficiently high enough to spread the magnetic flux over the circumferential surface, we may apply this model to actual iron cores.

In this way, we consider cylindrical solid iron-cores without upper and lower ends. First, we solve the three-dimensional of intensity with Laplace transforms and a Fourier expansion of boundary conditions. Next, magnetic reluctance is derived from the ratio between the magneto-motive force and the flux. The model described with Bessel functions is simplified in an approximated form. The applicability of the model is checked with experimental results.

SYMBOLS
a : Width of pole leg
b : Height of pole leg

$$c_{zm} = \frac{4}{\pi}\frac{1}{2m+1}\sin\left[\frac{\pi}{4}\frac{b}{z_m}(2m+1)\right]$$

$$c_{\theta n} = \frac{4}{\pi}\frac{1}{2n+1}\cos\left[\frac{\pi}{2}\frac{\theta_1}{\theta_2}(2n+1)\right]$$

H_r, H_θ, H_z : Magnetic intensity
h_r, h_θ, h_z : Normalized Laplace transform of $H(:,t)$
$j = \sqrt{-1}$: imaginary unit
m, n : Natural integer

$$p_n = \frac{\pi}{2\theta_2}(2n+1)$$

$$q_m = \frac{\pi}{2z_m}(2m+1)$$

R_1, R_2 : Inner, Outer radius of iron core
s : Variable of Laplace transform

z_m : Distance of spreading of magnetic intensity

$\alpha^2 = \mu\sigma s$

$\beta_m{}^2 = \alpha^2 + q_m{}^2$

μ : Permeability of iron core

μ_0 : Permeability of air ($4\pi \times 10^{-7}$ H/m)

θ_1 , θ_2 : A half of the angle between inner, outer sides of pole legs

σ : Conductivity of iron core

MAGNET CORE AND ASSUMPTIONS

Electromagnet and Iron core

Figure 1 shows the iron cores in the construction of an electromagnet; the outer, C-shaped iron core with rectangular pole legs is wound with magnet coils and the inner, cylindrical solid iron-core faces to the outer core with working air-gap. The magnetic flux enters the circumferential outer surface of the inner core, pole face, passes through circumferentially and goes out from the other pole face. The final object is to formulate the dynamical model of the magnetic force between the two iron cores; then, the primary subject is to model the relation between the incremental magnetic flux and the coil current.

A simple way to analyze the magnetic system is the application of the magnetic circuit theory. We consider that the electromagnetic system consists of the magnetic flux path that is a series connection of four paths in the inner and outer cores and in the two air-gaps. Then, we need the magnetic reluctances of the flux paths. Since the magnetic force varies with the coil current, the air-gap changes; hence the incremental magnetic force is a function of both the coil current and the air-gap length. If those increments are sufficiently small, then the linearized incremental force is given by the sum of the two incremental parts. The part of coil current is modeled with fixed air-gap; the part of air-gap length can be derived from the former result [2].

Experimental Data and Model Simplification

The outer core is made of laminated steel stacks of 0.2mm thick to exclude its dynamic characteristics and a =12mm, b =10mm, θ_1 =18.5deg. and θ_2 =41.5deg. The working air-gap is set to 1.0mm. A search coil of four turns is wound around the pole legs (two-turns in each) near their pole faces to detect the time-derivative of incremental flux to the coil current. Frequency response of the incremental flux is calculated by multiplying $1/j2\pi f$ (j is the imaginary unit and f is frequency) to the frequency response of the time-derivative.

The inner core of R_2 = 29mm is made of soft iron. To examine effects of the height, are selected 10 and 20mm: the same and twice as the outer core. The inner radii of 9.5 and 20mm are examined to see another effect. The bias coil current is 1.5A (flux density of 0.18T); the input voltage to the power amplifier with current feedback is sinusoidal functions with amplitude of 35% of the bias input. Figure 2 shows the frequency characteristics of the incremental flux

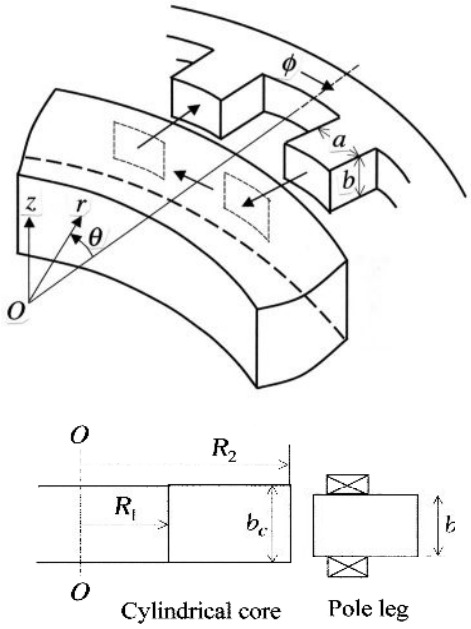

FIGURE 1: Magnet iron cores

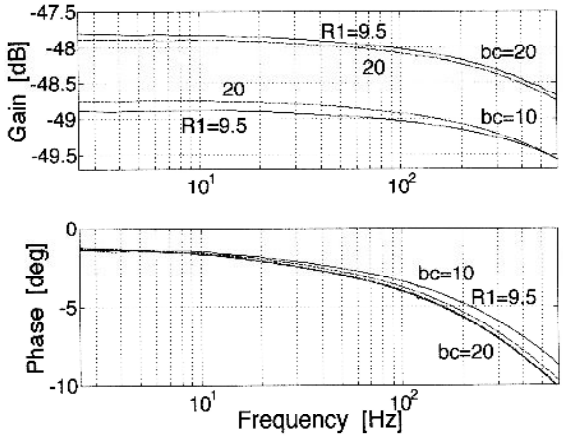

FIGURE 2: Frequency characteristics of incremental magnetic flux to coil current

to the coil current from 2.5Hz to 600Hz. We see that the difference due to the inner radius is negligible small, and that the effect of height is dynamically negligible small although the static gain is different.

Those results suggest that the upper and lower ends have a similar effect to the circumferential surface on the dynamics of the flux distribution, and that the range of the effective flux distribution is restrictive. This supports a simplification of modeling that we consider a core without ends.

Assumptions in Modeling

The assumptions and conditions for simplification are as follows:

(1) The cylindrical core is sufficiently high (axially long).

(2) Magnetic constants are uniform and constant. No magnetic saturation.
(3) No flux leakage.
(4) The fringing effects are neglected.
(5) The magnetic intensity is uniform and normal to the pole surfaces.
(6) Magnetomotive force on the surface is equal along any path between the two centering points of the pole faces.

EQUATIONS OF MAGNETIC FIELD

We take the coordinate system as in Figure 3: the origin at the intersection of the central axis of the inner core with the radial, central cross section of the outer core; the r axis in the radial direction; the θ axis in the circumferential direction with zero at the axial, central cross section of the outer core; and the z axis in the axial direction. Magnetic intensity H involved is described with those notations. The intensities are functions of r, θ, z and time, t; those arguments will be often omitted for simplicity.

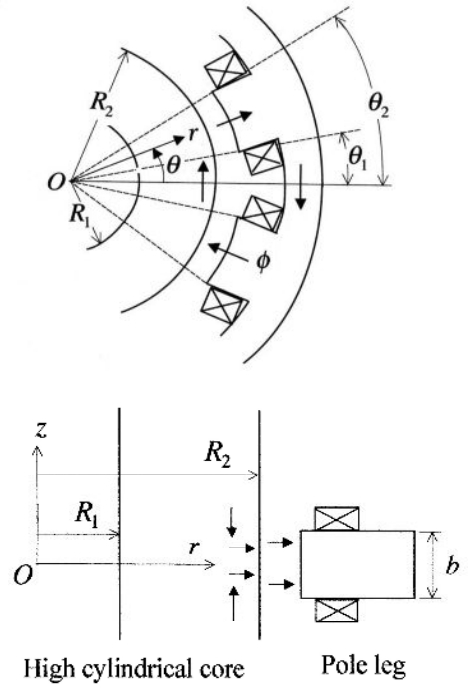

FIGURE 3: Coordinate system of high cylindrical core

Constraints and Boundary Conditions

The functions of the magnetic intensities are guessed in their form as follows:

(1) H_r is odd for θ, but even for z.
(2) H_θ is even for θ and z.
(3) H_z is odd for θ and z.

We give the boundary conditions as

$$H_r(R_1,\theta,z,t)=0 \tag{1}$$

$$H_r(R_2,\theta,z,t)=\begin{cases}-H_0(t), & -\theta_2\le\theta\le-\theta_1\\ 0, & -\theta_1<\theta<\theta_1\\ H_0(t), & \theta_1\le\theta\le\theta_2\end{cases},$$

$$-\frac{b}{2}<z<\frac{b}{2} \tag{2}$$

$$H_r(R_2,\theta,z,t)=0, \quad |z|>\frac{b}{2} \tag{3}$$

where $H_0(t)$ is the intensity assumed to be uniform on the surface. Assumption (6) is expressed as that the following function is constant for arbitrary z_c.

$$F_m=\int_0^{z_c}H_z(R_2,-\theta_c,z,t)dz+\int_{-\theta_c}^{\theta_c}H_\theta(R_2,\theta,z_c,t)R_2d\theta+\int_{z_c}^{0}H_z(R_2,\theta_c,z,t)dz,$$

$$\theta_c=\frac{1}{2}(\theta_1+\theta_2) \tag{4}$$

Fourier expansion of Boundary Conditions

We write eqs. (2) and (3) as

$$H_r(R_2,\theta,z,t)=H_0(t)g(\theta)f(z) \tag{5}$$

Then, we select the functions $g(\theta)$ and $f(z)$ as in Figures 4 and 5. Function $g(\theta)$ is expanded to the Fourier series with period $4\theta_2$ as

$$g(\theta)\cong\sum_{n=0}^{\infty}c_{\theta n}\sin(p_n\theta),$$

$$c_{\theta n}=\frac{4}{\pi}\frac{\cos(p_n\theta_1)}{2n+1}, \quad p_n=\frac{\pi}{2\theta_2}(2n+1) \tag{6}$$

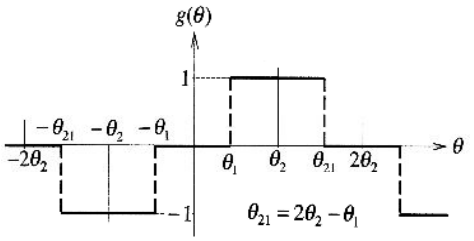

FIGURE 4: Circumferential function of Fourier expansion

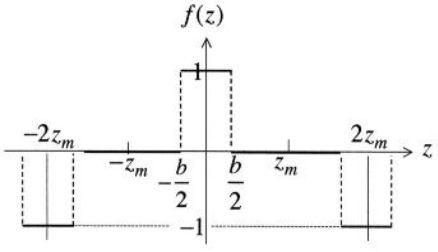

FIGURE 5: Axial function of Fourier expansion

In Figure 5, z_m is a distance of the distribution of the magnetic flux. This is unknown now; a way of its estimation will be discussed later. Function $f(z)$ is expanded with period $2z_m$ as

$$f(z) \cong \sum_{m=0}^{\infty} c_{zm} \cos(q_m z),$$

$$c_{zm} = \frac{4}{\pi} \frac{\sin\left(q_m \frac{b}{2}\right)}{2m+1}, \qquad q_m = \frac{\pi}{2z_m}(2m+1) \quad (7)$$

Equations of Intensity

If the magnetic constants, μ and σ, are uniform and constant, we have the following equations [4,5]

$$\nabla^2 H_r - \frac{1}{r^2} H_r - \frac{2}{r^2} \frac{\partial H_\theta}{\partial \theta} = \mu\sigma \frac{\partial H_r}{\partial t} \quad (8)$$

$$\nabla^2 H_\theta - \frac{1}{r^2} H_\theta + \frac{2}{r^2} \frac{\partial H_r}{\partial \theta} = \mu\sigma \frac{\partial H_\theta}{\partial t} \quad (9)$$

$$\nabla^2 H_z = \mu\sigma \frac{\partial H_z}{\partial t} \quad (10)$$

$$\frac{1}{r}\left(H_r + r\frac{\partial H_r}{\partial r} + \frac{\partial H_\theta}{\partial \theta} \right) + \frac{\partial H_z}{\partial z} = 0 \quad (11)$$

where

$$\nabla^2 = \frac{\partial^2}{\partial r^2} + \frac{1}{r}\frac{\partial}{\partial r} + \frac{1}{r^2}\frac{\partial^2}{\partial \theta^2} + \frac{\partial^2}{\partial z^2} \quad (12)$$

Equation (11) is the continuity equation of the flux density.

Variables H_r and H_θ are simultaneous in eqs. (8) and (9). Equation (10) of H_z is independent of the others. If we substitute the term $\partial H_\theta / \partial \theta$ obtained from eq. (11) into eq. (8), we have the equation excluding H_θ as

$$\nabla^2 H_r + \frac{2}{r}\frac{\partial H_r}{\partial r} + \frac{1}{r^2} H_r + \frac{2}{r}\frac{\partial H_z}{\partial z} = \mu\sigma \frac{\partial H_r}{\partial t} \quad (13)$$

Hence, it seems simple to solve eq. (10) first, and then to solve eq. (13). In this case, we can obtain a solution of H_θ from eq. (11) without solving eq. (9).

Solution with Laplace Transform

We use the Laplace transforms of the variables with their initial values of zero as

$$\bar{H}_r(r,\theta,z,s) = \bar{H}_0(s) h_r(r,\theta,z,s),$$
$$\bar{H}_\theta(r,\theta,z,s) = \bar{H}_0(s) h_\theta(r,\theta,z,s),$$
$$\bar{H}_z(r,\theta,z,s) = \bar{H}_0(s) h_z(r,\theta,z,s) \quad (14)$$

where $\bar{H}_0(s)$ is the Laplace transform of $H_0(t)$. Then, eqs. (10), (13) and (11) are transformed to

$$\frac{\partial^2 h_z}{\partial r^2} + \frac{1}{r}\frac{\partial h_z}{\partial r} + \frac{1}{r^2}\frac{\partial^2 h_z}{\partial \theta^2} + \frac{\partial^2 h_z}{\partial z^2} - \alpha^2 h_z = 0 \quad (15)$$

$$\frac{\partial^2 h_r}{\partial r^2} + \frac{3}{r}\frac{\partial h_r}{\partial r} + \frac{1}{r^2}\frac{\partial^2 h_r}{\partial \theta^2} + \frac{\partial^2 h_r}{\partial z^2} + \left(\frac{1}{r^2} - \alpha^2\right) h_r$$
$$= -\frac{2}{r}\frac{\partial h_z}{\partial z} \quad (16)$$

$$\frac{1}{r}\left(h_r + r\frac{\partial h_r}{\partial r} + \frac{\partial h_\theta}{\partial r} \right) + \frac{\partial h_z}{\partial z} = 0 \quad (17)$$

where

$$\alpha^2 = \mu\sigma s \quad (18)$$

The boundary conditions of eqs. (1) and (5) become

$$h_r(R_1,\theta,z,s) = 0 \quad (19)$$

$$h_r(R_2,\theta,z,s) = g(\theta) f(z) \quad (20)$$

The condition of eq. (4) can be replaced by

$$\frac{\partial}{\partial \theta} h_z(R_2,-\theta,z,s) + R_2 \frac{\partial}{\partial z} h_\theta(R_2,\theta,z,s) = 0 \quad (21)$$

First, we solve eq. (15) with separation of variables. Considering the form, we obtain a solution

$$h_z = \sum_{n,m} A_{nm}(u_n, r) \sin(v_m z) \sin(u_n \theta) \quad (22)$$

where u_n and v_m are parameters, and

$$A_{nm}(\nu, r) = c_{z1nm} J_\nu(j\gamma_m r) + c_{z2nm} Y_\nu(j\gamma_m r),$$
$$\gamma_m{}^2 = \alpha^2 + v_m{}^2 \quad (23)$$

where c_{z1nm} and c_{z2nm} are constants, and J_ν and Y_ν are Bessel functions of the first and second and order ν.

Substituting eq. (22) into (16), we obtain a particular solution

$$h_{rs} = \sum_{n,\ m} \frac{q_m}{j\gamma_m} A_{nm}(u_n - 1, r) \cos(v_m z) \sin(u_n \theta) \quad (24)$$

where we used the following relation

$$\frac{dN_\nu(\beta r)}{dr} = \beta N_{\nu-1}(\beta r) - \frac{\nu}{r} N_\nu(\beta r) \quad (25)$$

for a Bessel function $N_\nu(\beta r)$ [6]:

Next,, we get a homogeneous solution of eq. (16) with $\partial h_z / \partial z = 0$ as

$$h_{rh} = \frac{1}{r} \sum_{n,m} A_{2nm}(u_{2n}, r) \cos(v_{2m} z) \sin(u_{2n} \theta) \quad (26)$$

where u_{2n} and v_{2m} are parameters, and

$$A_{2nm}(\nu, r) = c_{21nm} J_\nu(j\gamma_{2m} r) + c_{22nm} Y_\nu(j\gamma_{2m} r),$$
$$\gamma_{2m}{}^2 = \alpha^2 + v_{2m}{}^2 \quad (27)$$

where c_{21nm} and c_{22nm} are constants. A solution of eq. (16) is given by $h_r = h_{rh} + h_{rs}$.

From the boundary conditions of eqs. (19) and (20), and setting $u_{2n} = u_n = p_n$ and $v_{2m} = v_m = q_m$, we have

$$h_r = \sum_{n,m} \left[\frac{R_2}{r} d_{nm} M_{nm}(r) + d_{znm} N_{nm}(r) \right] \cdot \cos(q_m z) \sin(p_n \theta) \quad (28)$$

where

$$M_{nm}(r)=\frac{J_{pn}(j\beta_m r)}{J_{pn}(j\beta_m R_1)}-\frac{Y_{pn}(j\beta_m r)}{Y_{pn}(j\beta_m R_1)},$$

$$N_{nm}(r)=\frac{J_{pn-1}(j\beta_m r)}{J_{pn-1}(j\beta_m R_1)}-\frac{Y_{pn-1}(j\beta_m r)}{Y_{pn-1}(j\beta_m R_1)} \quad (29)$$

$$\beta_m{}^2=\alpha^2+q_m{}^2 \quad (30)$$

and d_{nm} and d_{znm} are constants satisfying the relation

$$Md_{nm}+Nd_{znm}=c_{zm}c_{\theta n} \quad (31)$$

where

$$M=M_{nm}(R_2),\quad N=N_{nm}(R_2) \quad (32)$$

In this case, eq. (22) is rewritten as

$$h_z=\sum_{n,m}\frac{j\beta_m}{q_m}d_{znm}L_{nm}(r)\sin(q_m z)\sin(p_n\theta) \quad (33)$$

where

$$L_{nm}(r)=\frac{J_{pn}(j\beta_m r)}{J_{pn-1}(j\beta_m R_1)}-\frac{Y_{pn}(j\beta_m r)}{Y_{pn-1}(j\beta_m R_1)} \quad (34)$$

Finally, a solution of h_θ is obtained from eq. (17) as

$$h_\theta=\sum_{n,m}\left[\frac{R_2}{p_n}d_{nm}\frac{dM_{nm}(r)}{dr}+d_{znm}N_{nm}(r)\right]\cdot\cos(q_m z)\cos(p_n\theta) \quad (35)$$

where

$$\frac{dM_{nm}(r)}{dr}=j\beta_m K_{nm}(r)-\frac{p_n}{R_2}M_{nm}(r) \quad (36)$$

$$K_{nm}(r)=\frac{J_{pn-1}(j\beta_m r)}{J_{pn}(j\beta_m R_1)}-\frac{Y_{pn-1}(j\beta_m r)}{Y_{pn}(j\beta_m R_1)} \quad (37)$$

Determination of Constants

The other equation to determine two constants is given by eq. (21) as

$$\frac{R_2}{p_n}A_1 d_{nm}+\left[N+\frac{j\beta_m p_n}{R_2 q_m{}^2}L\right]d_{znm}=0 \quad (38)$$

where

$$A_1=\left.\frac{dM_{nm}(r)}{dr}\right|_{r=R_2}=j\beta_m K-\frac{p_n}{R_2}M \quad (39)$$

$$K=K_{nm}(R_2),\quad L=L_{nm}(R_2) \quad (40)$$

From eqs. (31) and (38) we have the constants

$$d_{nm}=\frac{c_{zm}c_{\theta n}}{M}\frac{-D_{nm}}{1-D_{nm}},$$

$$d_{znm}=\frac{c_{zm}c_{\theta n}}{N}\frac{1}{1-D_{nm}} \quad (41)$$

where

$$D_{nm}=\frac{\frac{j\beta_m p_n}{R_2 q_m{}^2}\frac{L}{N}+1}{\frac{j\beta_m R_2}{p_n}\frac{K}{M}-1} \quad (42)$$

MAGNETIC RELUCTANCE

Expression of Reluctance

We calculate the magnetomotive force between the centers of the two pole faces, f_m, by

$$f_m(\theta_c)=\int_{-\theta_c}^{\theta_c}h_\theta(R_2,\theta,0,s)R_2 d\theta \quad (43)$$

Then, we consider the mean force $\bar{f}_m$ by

$$\bar{f}_m=\frac{1}{\theta_2-\theta_1}\int_{\theta_1}^{\theta_2}f_m(\theta)d\theta \quad (44)$$

This is written as

$$\bar{f}_m=\frac{2R_2}{\theta_2-\theta_1}\sum_{n=0}\frac{c_{\theta n}}{p_n{}^3}\cos(p_n\theta_1)\sum_{m=0}j\beta_m R_2 c_{zm}A_{nm} \quad (45)$$

where

$$A_{nm}=\frac{\frac{K}{M}-\frac{p_n}{j\beta_{nm}R_2}}{1-\left[\frac{K}{M}-\frac{2p_n}{j\beta_m R_2}\right]\left(\frac{q_m R_2}{p_n}\right)^2\frac{N}{L}} \quad (46)$$

We estimate the reluctance R_m by the ratio of the magnetonitive force F_m to the total magnetic flux Φ. From $F_m=H_0(s)\bar{f}_m$ and $\Phi=\mu H_0(s)ab$, we have

$$R_m=\frac{\bar{f}_m}{\mu ab} \quad (475)$$

In this equation $\bar{f}_m$ expresses the equivalent length of the flux path.

Estimation of Effective Height

The effective distance of the spreading flux, z_m, can be estimated from the flux continuity between the pole face and the $r-z$ plain of $\theta=0$. Unfortunately, this method is not simple here because it needs an integral calculation of Bessel functions that is complicated. Instead, we seek a value that gives a saturated value of the reluctance. Several examples give a rough relation

$$z_m\cong\frac{3}{2}R_2\theta_2 \quad (48)$$

Approximation for Terms of Bessel Functions

Numerical calculation of Bessel function is complicated and may not go well in ill cases. To avoid such cases, we consider an approximation. First, we use the first kind of Hankel function instead of the second kind of Bessel function for computational convenience; in the below, $Y_\nu(\cdot)$

is replaced by $H_\nu(\cdot) = H_\nu^1(\cdot)$.

For complex non-zero numbers z_1 and z_2, and a positive real number ν, we define the functions

$$P_\nu = \frac{J_\nu(z_2)}{J_\nu(z_1)} - \frac{H_\nu(z_2)}{H_\nu(z_1)},$$

$$Q_\nu = \frac{J_{\nu-1}(z_2)}{J_\nu(z_1)} - \frac{H_{\nu-1}(z_2)}{H_\nu(z_1)},$$

$$T_\nu = \frac{J_{\nu+1}(z_2)}{J_\nu(z_1)} - \frac{H_{\nu+1}(z_2)}{H_\nu(z_1)} \tag{49}$$

Several examples support the following approximations:

$$\frac{Q_\nu}{P_\nu} \cong \frac{1}{\tan\left(z_2/(\nu\lambda_{z\nu})\right)} + \frac{\nu}{z_2} \quad \text{for} \quad \nu > 1 \tag{50}$$

$$\frac{T_\nu}{P_\nu} \cong \frac{-1}{\tan\left(z_2/(\nu\lambda_{z\nu})\right)} + \frac{\nu}{z_2} \quad \text{for} \quad \nu > 0 \tag{51}$$

where

$$\lambda_{z\nu} = \frac{k_{z\nu}+1}{k_{z\nu}-1}, \qquad k_{z\nu} = \left(\frac{z_2}{z_1}\right)^{2\nu} \tag{52}$$

We can use these approximation if $\theta_2 < \pi/2$ because then $p_0 > 1$. In addition, in higher frequencies, we have a simple expression

$$\bar{f}_{m\infty} = (\alpha R_2) l_{m\infty} \tag{53}$$

where

$$l_{m\infty} = \frac{2R_2}{\theta_2 - \theta_1} \sum_{n=0}^{\infty} \frac{c_{\theta n}}{p_n} \cos(p_n\theta_1) \sum_{m=0}^{\infty} \frac{c_{zm}}{{p_n}^2 + (q_m R_2)^2} \tag{54}$$

CHECK OF THE MODEL

We take the core of b_c =10mm and R_1 =20mm; the frequency response in Fig.2 is shown again with the filled lines in Fig. 6. Neglecting the reluctance of the laminated outer core, we calculate the numerical result with $s = j2\pi f$ from the equation

$$\frac{\Phi(s)}{I(s)} = \frac{\mu_0 A_0 N}{2l_0} \frac{1}{1 + \frac{\mu_0}{\mu}\frac{\bar{f}_{m\infty}(s)}{2l_0}} \tag{55}$$

where A_0 is an effective area of the air-gap, N the turns of magnet coil, l_0 the air-gap length. For the inner core taken here, we guess as

$$A_0 = \left(a + \frac{3}{2}l_0\right)(b + l_0) \tag{56}$$

considering the fringing effects. The other constants used are

$\mu = 5,000\mu_0$ H/m, $\quad \sigma = 1.0 \times 10^7$ 1/ Ωm

$N = 200$

The numerical gain adjusted by the sensor gain is shifted 0.1dB down to simplify the comparison and is shown by the dashed lines in the figure. The dynamical difference in the gain is small, about 0.1dB; however, the difference is large in the phase. This seems due to other factors not considered in the model, mainly, static hysteresis and flux saturation.

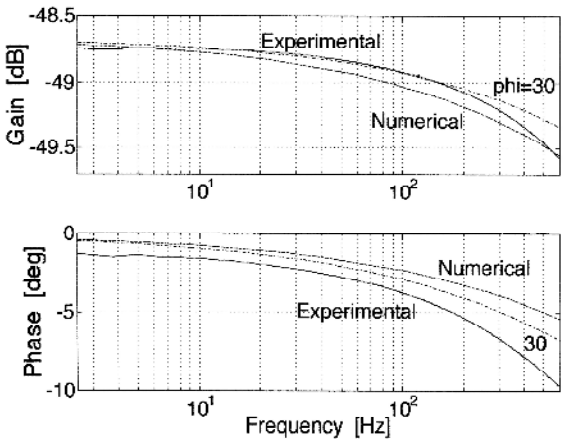

FIGURE 6: Numerical and experimental results

We note the numerical result may be better if we assume a complex permeability in the form

$$\mu' = \mu e^{-j\varphi} \tag{57}$$

The dash-dot lines give the result with φ =30deg.

CONCLUSIONS

We considered a high cylindrical solid iron-core where magnetic flux spreads over the circumferential surface, and we presented an analytical model of the magnetic reluctance. The model obtained by a series of Bessel functions was approximated by a simple series without the Bessel functions. The numerical result was compared with the experimental data to check the usefulness of the model.

ACKNOWLEDGMENTS

I thank Nippon Steel Corporation for providing silicon steel strips.

REFERENCES

1. Feeley, J. J., A Simple Dynamic Model for Eddy Currents In a Magnetic Actuator, *IEEE Trans. on Magnetics*, Vol. 32, No.2, pp.453-458, 1996.
2. Fukata, S., A Frequency-Domain Model of Electromagnetic Actuators Composed of Solid Iron Cores, *JSME Int. Journal*, Vol. C-43, No. 1, pp.38-46, 2000.
3. Fukata, S., Analytical Model of Magnetic Reluctance in Plain Solid Iron Cores, Tranns. of Japan AEM (in Japanese), Vol.15, No. 3, pp. 325-332, 2007.
4. Stoll, R.L., *The Analysis of eddy currents*, pp. 4-6, Clarendoon Press, 1974.
5. Umoto, S., *Electromagnetics* (in Japanse), pp.17-18, Shokodo, 1993.
6. Moriguchi S., Udagawa K., and Hitotsumatsu, S., Mathematical Formulas Ⅲ (in Japanese), Iwanamishoten, pp. 145-162, 1984.